AMERICAN SOCIETY FOR MICROBIOLOGY | Applied and Environmental Microbiology®

ENZYMOLOGY AND PROTEIN ENGINEERING

A Haloalkane Dehalogenase from *Saccharomonospora viridis* Strain DSM 43017, a Compost Bacterium with Unusual Catalytic Residues, Unique (*S*)-Enantiopreference, and High Thermostability

Klaudia Chmelova,[a,b] Eva Sebestova,[a] Veronika Liskova,[a] Andy Beier,[a] David Bednar,[a] Zbynek Prokop,[a] Radka Chaloupkova,[a] Jiri Damborsky[a,b]

[a]Loschmidt Laboratories, Department of Experimental Biology and RECETOX, Masaryk University, Brno, Czech Republic
[b]International Clinical Research Center, St. Anne's Universty Hospital, Brno, Czech Republic

ABSTRACT Haloalkane dehalogenases can cleave a carbon-halogen bond in a broad range of halogenated aliphatic compounds. However, a highly conserved catalytic pentad composed of a nucleophile, a catalytic base, a catalytic acid, and two halide-stabilizing residues is required for their catalytic activity. Only a few family members, e.g., DsaA, DmxA, or DmrB, remain catalytically active while employing a single halide-stabilizing residue. Here, we describe a novel haloalkane dehalogenase, DsvA, from a mildly thermophilic bacterium, *Saccharomonospora viridis* strain DSM 43017, possessing one canonical halide-stabilizing tryptophan (W125). At the position of the second halide-stabilizing residue, DsvA contains the phenylalanine F165, which cannot stabilize the halogen anion released during the enzymatic reaction by a hydrogen bond. Based on the sequence and structural alignments, we identified a putative second halide-stabilizing tryptophan (W162) located on the same α-helix as F165, but on the opposite side of the active site. The potential involvement of this residue in DsvA catalysis was investigated by the construction and biochemical characterization of the three variants, DsvA01 (F165W), DsvA02 (W162F), and DsvA03 (W162F and F165W). Interestingly, DsvA exhibits a preference for the (*S*)- over the (*R*)-enantiomers of β-bromoalkanes, which has not been reported before for any characterized haloalkane dehalogenase. Moreover, DsvA shows remarkable operational stability at elevated temperatures. The present study illustrates that protein sequences possessing an unconventional composition of catalytic residues represent a valuable source of novel biocatalysts.

IMPORTANCE The present study describes a novel haloalkane dehalogenase, DsvA, originating from a mildly thermophilic bacterium, *Saccharomonospora viridis* strain DSM 43017. We report its high thermostability, remarkable operational stability at high temperatures, and an (*S*)-enantiopreference, which makes this enzyme an attractive biocatalyst for practical applications. Sequence analysis revealed that DsvA possesses an unusual composition of halide-stabilizing tryptophan residues in its active site. We constructed and biochemically characterized two single point mutants and one double point mutant and identified the noncanonical halide-stabilizing residue. Our study underlines the importance of searching for noncanonical catalytic residues in protein sequences.

KEYWORDS haloalkane dehalogenase, (*S*)-enantiopreference, thermophilic bacterium, catalytic residues, halide-stabilizing residues, dehalogenase, enantioselectivity, haloalkane, kinetics, mutagenesis, structure, substrate specificity, thermostability

Citation Chmelova K, Sebestova E, Liskova V, Beier A, Bednar D, Prokop Z, Chaloupkova R, Damborsky J. 2020. A haloalkane dehalogenase from *Saccharomonospora viridis* strain DSM 43017, a compost bacterium with unusual catalytic residues, unique (*S*)-enantiopreference, and high thermostability. Appl Environ Microbiol 86:e02820-19. https://doi.org/10.1128/AEM.02820-19.

Editor Hideaki Nojiri, University of Tokyo

Address correspondence to Jiri Damborsky, jiri@chemi.muni.cz.

Received 4 December 2019
Accepted 8 June 2020
Accepted manuscript posted online 19 June 2020
Published 18 August 2020

Haloalkane dehalogenases (HLDs, EC 3.8.1.5) are predominantly microbial enzymes that catalyze the hydrolytic conversion of a broad range of halogenated aliphatic compounds to primary alcohol, a halide ion, and a proton (1, 2). The two-step reaction mechanism (Fig. 1) is initiated by a nucleophilic attack of aspartic acid on a carbon atom of the substrate, resulting in a covalent alkyl-enzyme intermediate. This complex is subsequently hydrolyzed by a water molecule activated by the catalytic base (3). Structurally, HLDs belong to the superfamily of α/β-hydrolases and consist of a conserved main domain and a variable cap domain. Active sites of the HLDs are buried in hydrophobic cavities at an interface between these two domains and are connected with the protein surface by several access tunnels (4–6). The active sites of HLDs typically contain five catalytically relevant residues: (i) nucleophilic aspartate, (ii) basic histidine, (iii) catalytic aspartic or glutamic acid, and (iv and v) two halide-stabilizing residues that differ among the individual members of HLDs. While the halide-stabilizing residues of HLD-I members are formed by a Trp-Trp pair, HLD-II members employ Asn/Gln-Trp/Tyr and HLD-III members use Asn-Trp residues (7). These primary halide-stabilizing residues are known to stabilize the halogen atom of the substrate in the activated complex and the released halide anion via the formation of two hydrogen bonds (3, 8, 9). The importance of these residues for the catalytic function was confirmed by several independent experiments covering site-directed mutagenesis, steady-state fluorescence quenching, stopped-flow fluorescence, and steady-state enzyme kinetics (8–14). Other nearby amino acids can also contribute to the course of dehalogenase reaction via electrostatic interactions. However, these residues are not essential for the catalysis since they do not make a hydrogen bond with the halogen atom and the halide ion (8). Despite the claimed necessity of two halide-stabilizing residues for HLDs to function (3, 8, 15), the ability to hydrolyze halogenated compounds was recently also described for enzymes with just a single primary halide-stabilizing residue: DsaA (16), DmxA (17), and DmrB (18).

Here, we describe the biochemical characterization of a novel haloalkane dehalogenase, DsvA, originating from the mildly thermophilic bacterium *Saccharomonospora viridis* strain DSM 43017 (19, 20). The thermophilic origin results in higher thermodynamic and operational stability compared to other HLDs. Interestingly, the enzyme exhibits unique (*S*)-enantiopreference toward β-substituted brominated alkanes, which has not been previously observed for any other HLD. A sequence alignment (Fig. S1 in the supplemental material) initially suggested that DsvA possesses only one halide-stabilizing tryptophan instead of the two tryptophan residues typical for most HLD-I members. The structural comparison of a DsvA homology model with the crystal structure of a closely related representative member DmrA (Fig. 2) uncovered a putative second halide-stabilizing tryptophan located on the opposite side of the catalytic pocket from the usual position of the second halide-stabilizing residue in other HLD-I members characterized to date. This noncanonical arrangement of the halide-stabilizing residues might affect the binding of halogenated substrates to the enzyme active site and thus may have an impact on the enzyme activity, substrate specificity, and enantioselectivity. Therefore, we constructed three DsvA variants, DsvA01 (F165W), DsvA02 (W162F), and DsvA03 (W162F+F165W) with a modified arrangement of the halide-stabilizing residues in order to better understand their importance for the catalysis.

RESULTS

Identification of putative haloalkane dehalogenases. Sequence similarity searches against the non-redundant (nr) database of NCBI (21) led to the identification of 5,657 sequences. This sequence set was clustered to distinguish HLDs from other related proteins. The HLD cluster (Fig. S2) was composed of 978 nonunique sequences originating from 1,098 different sources, including unclassified organisms and artificial constructs. Four putative HLDs were identified in the genomes of four thermophilic organisms: *S. viridis* DSM 43017 (accession number WP_012795647), *Isosphaera pallida* ATCC 43644 (WP_013564874), *Chloroflexus aggregans* DSM 9485 (WP_012615857), and

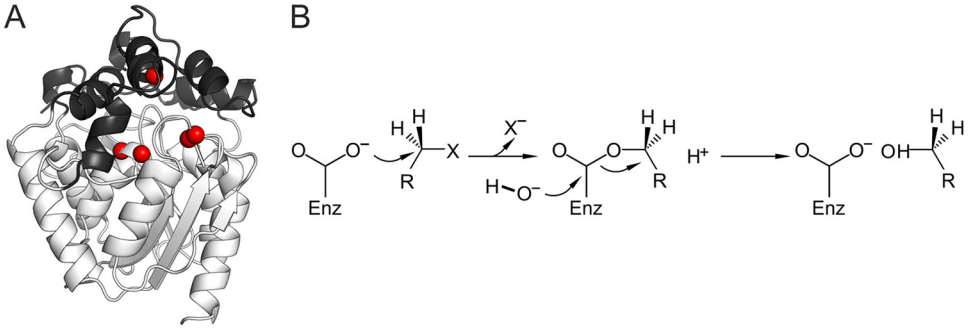

FIG 1 (A) Overview of the tertiary structure of HLDs consisting of a conserved main domain (white) and the variable cap domain (black) with the active site located at the interface between these two domains. Catalytic residues are represented by red balls. (B) Scheme of the reaction mechanism of HLDs (2).

Chloroflexus aurantiacus J-10-fl (WP_012259370). DsvA from *S. viridis* DSM 43017 was classified to the HLD-I subfamily, while the other three putative HLDs to the HLD-III subfamily. DsvA was selected for further biochemical characterization because most of the HLD-III members have been reported as difficult to prepare or poorly soluble proteins (18, 22, 23).

Phylogenetic and structural analyses based on the homology model of DsvA. Among the HLD-I members, DsvA showed the highest protein sequence identity (80%) with DsaA (16), whose crystal structure is not available, followed by DmrA (55%) (18) and DpcA (51%) (24). Sequence alignment of the selected HLD-I members revealed that DsvA and DsaA (16) possess only one halide-stabilizing residue (W125). In the position of the second tryptophan (Fig. S1), both of these enzymes contain phenylalanine (F165). However, a nearby tryptophan at position 162 (W162), where there is a phenylalanine in the majority of other HLD-I members, could potentially play the role of the second halide-stabilizing residue in DsvA. A homology model of DsvA was built using the crystal structure of closely related DmrA (18). The alignment of both DmrA template and the structural model of DsvA resulted in a root mean square deviation (RMSD) of Cα atoms of 0.1 Å. The structural comparison revealed that the majority of catalytic residues of DsvA are located in the same position as the corresponding residues in

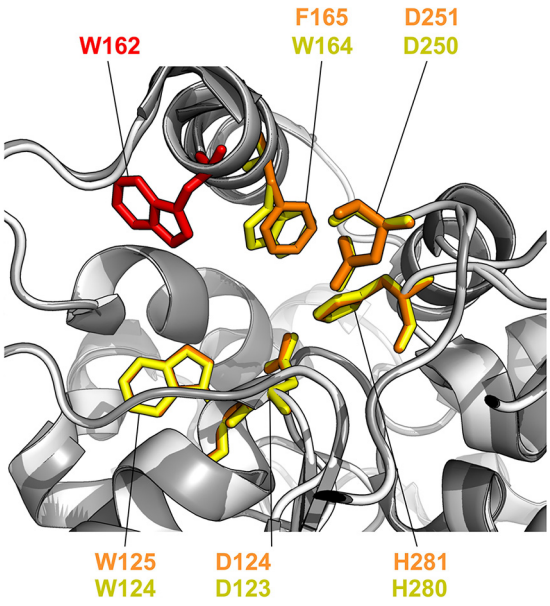

FIG 2 The active sites of DmrA (white) and DsvA (gray) with highlighted catalytic residues of DmrA (yellow) and DsvA (orange). The putative second halide-stabilizing residue of DsvA (W162) is shown in red.

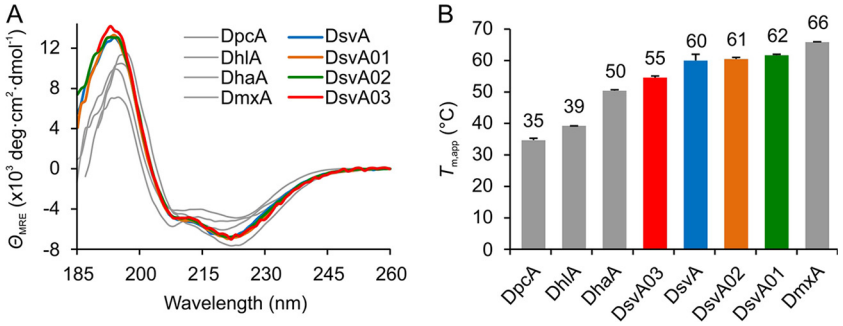

FIG 3 Comparison of CD spectra (A) and apparent melting temperatures (B) of DsvA and its variants with selected representative members of subfamilies HLD-I (DpcA and DhlA) and HLD-II (DhaA and DmxA).

DmrA (18), with the exception of the putative second halide-stabilizing tryptophan (W162). Although the tryptophan W162 (Fig. 2) is located at the same α-helix as F165, its side chain is oriented on the opposite side from the side chain of the phenylalanine. The residue W162 could form a hydrogen bond with the halogen atom of the substrate and thus contribute to the enzyme catalysis, but the stabilization will come from the opposite side compared with the position of the usual second halide-stabilizing residue. To further analyze the involvement of W162 and F165 in DsvA catalysis, two single point mutants, DsvA01 and DsvA02, carrying F165W and W162F substitutions, respectively, and one double point mutant, DsvA03, carrying a combination of both substitutions, were constructed and their properties were compared with those of the wild type, DsvAwt.

Correct folding and thermostability. The sequence of the *dsvA* gene was optimized for heterologous expression in *Escherichia coli* and *de novo* synthesized. Three variants, DsvA01 (F165W), DsvA02 (W162F), and DsvA03 (W162F+F165W), were constructed by site-directed mutagenesis. The proteins were expressed in *E. coli* BL21(DE3) cells and purified to homogeneity, with a comparable average yield of 80 to 120 mg per liter of cell culture and purity of $\geq$90% (Fig. S3). Basic biochemical characterization of DsvAwt, including the determination of its operational stability at elevated temperature, pH profile, and steady-state kinetic parameters are presented in the supplemental material (Fig. S4, Tables S1 and S2, Methods S1 to S3, and Results S1 to S3). The proper folding of DsvA variants was verified by circular dichroism (CD) spectroscopy. Similar to other related HLDs, DsvA and its variants exhibited CD spectra with one positive peak at 195 nm and two negative maxima at 208 and 221 nm, a characteristic of α-helical content (4–6, 25), suggesting correct folding of the enzymes (Fig. 3). Thermally induced denaturation of DsvA variants was tested by monitoring their ellipticity at 221 nm at an elevated temperature. The determined apparent melting temperature ($T_{m,app}$) of DsvA, 60.0 $\pm$ 1.0°C, was slightly higher than the apparent melting temperatures observed for most of the characterized HLD-I and HLD-II members, ranging from 34 to 59°C (26–29). A higher apparent melting temperature than for DsvA was thus far observed only for DmxA ($T_{m,app}$ = 65.9 $\pm$ 0.1°C), although surprisingly, this enzyme was isolated from the psychrophilic bacterium *Marinobacter* sp. ELB17 (17). While both DsvA01 and DsvA02 exhibited similar apparent melting temperatures (61.7 $\pm$ 0.2°C and 60.5 $\pm$ 0.5°C, respectively) as DsvA, the apparent melting temperature of DsvA03 (54.8 $\pm$ 0.5°C) was lower by 5°C (Fig. 3).

Substrate specificity. The substrate specificity profiles of DsvA, DsvA01, and DsvA02 were investigated with the set of 30 different halogenated compounds (Fig. 4 and Table S3), while the activity of DsvA03 was verified with the representative substrate 1,2-dibromoethane. DsvA, DsvA01, and DsvA02 exhibited better activities toward terminally substituted brominated and iodinated substrates with an alkyl chain length of six carbon atoms than toward the chlorinated ones. The highest activity of DsvA was observed with 1-bromohexane (0.06785 μmol $\cdot$ s^{-1} $\cdot$ mg^{-1}; labeled as

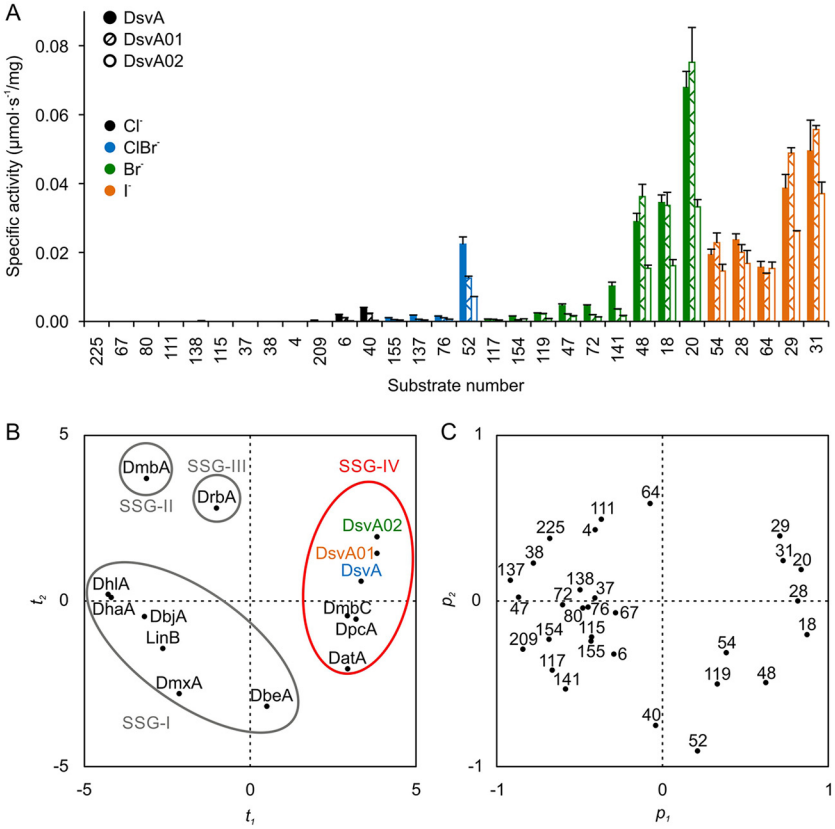

FIG 4 The substrate specificities of DsvA, DsvA01, and DsvA02. (A) The substrate specificity profiles determined with 30 halogenated compounds. (B) The score plot t_1/t_2 from PCA with a transformed data set representing a two-dimensional window into the multidimensional space, where the objects (enzymes) with similar properties (specificity profiles) are collocated. The t_1/t_2 score plot describing 48.5% of the variance in the data set shows the clustering of HLDs into individual substrate specificity groups (SSGs). DsvA variants were clustered into SSG-IV. (C) The corresponding loading plot p_1/p_2 from PCA showing the substrates that govern the clustering of enzymes into individual SSGs. The numbering of the substrates is provided in Table S3 in the supplemental material.

substrate no. 20 in Fig. 4). No significant difference was observed between the activities of DsvA01 and DsvA. On the contrary, DsvA02 exhibited a 30% to 50% drop in activity toward most of the tested halogenated substrates (Fig. 4 and Table S3), suggesting that W162 is involved in stabilization of halogenated substrates during the catalytic cycle. The specific activity of DsvA03 toward 1,2-dibromoethane (0.00105 μmol·s^{-1}·mg^{-1}) was similar to that of DsvA02 (0.00143 μmol · s^{-1} · mg^{-1}). The principal-component analysis (PCA) was performed to compare the overall activity quantitatively and substrate specificity of DsvA, DsvA01, and DsvA02 with other characterized HLDs. Due to the preference for terminally substituted brominated and iodinated compounds, all analyzed DsvA variants were clustered into the substrate specificity group IV (Fig. 4), together with the wild-type enzymes DmbC, DpcA, and DatA (30).

Enantioselectivity. Enantioselectivity of DsvA variants was assessed by determining the kinetic resolution toward representatives of three substrate groups: (i) racemic β-brominated alkanes (2-bromopentane and 2-bromohexane), selected based on the preference of DsvA toward long brominated substrates; (ii) α-brominated ester (ethyl-2-bromopropionate), chosen due to high enantioselectivity of other HLDs toward this substrate (31–33); and (iii) α-brominated amide (*N*-butyl-2-bromopropionamide), selected for its importance as a precursor for medicinal chemistry (34). Very low enantioselectivity of DsvAwt was observed in the reaction with both β-brominated alkanes (Table 1 and Fig. S5). Strikingly, DsvAwt exhibited preference toward (*S*)-2-bromopentane and (*S*)-2-bromohexane, whereas all other characterized HLDs show prefer-

TABLE 1 Enantioselectivity of DsvA, DsvA01, DsvA02, and DsvA03 toward 2-bromopentane, 2-bromohexane, ethyl-2-bromopropionate, and *N*-butyl-2-bromopropionamide

Substrate	Temp (°C)	*E* value[b]			
		DsvA	DsvA01	DsvA02	DsvA03
2-Bromopentane[a]	20	4	4	6	7
2-Bromohexane[a]	20	4	-	-	-
Ethyl-2-bromopropionate	20	1	5	2	5
N-Butyl-2-bromopropionamide	37	13	9	3	-

[a](*S*)-Enantiopreference was identified for DsvA variants in the reaction with 2-bromopentane and 2-bromohexane, for which the standards were available.
[b]*E* value is defined as the ratio between the specificity constants (k_{cat}/K_m) for the two enantiomers; see equation 2 in the Materials and Methods section. -, not determined.

ence for the (*R*)-enantiomer of the substrates (24, 26, 28, 29, 31). The same enantiopreference, as well as similar enantioselectivity (*E* values ranging from 4 to 7) toward 2-bromopentane, was detected for all constructed DsvA variants (DsvA01, DsvA02, and DsvA03) regardless of different arrangement of their halide-stabilizing residues. This observation indicates that enantiodiscrimination of β-brominated alkanes by DsvA is also driven by structural features other than the different binding of the two enantiomers via two hydrogen-binding interactions with the side chains of the halide-stabilizing residues.

In contrast, interesting changes in enantioselectivity of DsvA toward the tested α-brominated ester (ethyl-2-bromopropionate) were observed after modification of its halide-stabilizing residues (Table 1 and Fig. S5). DsvAwt exhibited no enantioselectivity toward ethyl-2-bromopropionate, while most of the HLDs are highly enantioselective toward this substrate (31). The introduction of the F165W mutation into DsvA01 induced a small but significant ability to discriminate between the two enantiomers of the ester (*E* value = 5). A negligible increase in the enzyme enantioselectivity was also observed after the introduction of W162F or W162F+F165W into DsvA02 and DsvA03, respectively.

The most pronounced effect of modification of halide-stabilizing residues was observed in the reaction of DsvA with *N*-butyl-2-bromopropionamide (Table 1 and Fig. S5). While the highest enantioselectivity toward the amide was exhibited by DsvAwt (*E* value = 13), the introduction of the F165W mutation into DsvA01 caused a decrease of the enzyme enantioselectivity (*E* value = 9). A more pronounced decrease in enantioselectivity toward the same substrate (*E* value = 3) was observed when the second halide-stabilizing residue W162 was replaced by phenylalanine in DsvA02, implying that the type of halide-stabilizing residues, as well as their geometric arrangement inside the enzyme active site, are important determinants of enantiodiscrimination of α-brominated amide by DsvA.

Molecular docking of β-bromoalkanes into the active site. In order to get a more in-depth insight into the (*S*)-enantiopreference of DsvA toward the β-brominated alkanes, the individual enantiomers of the 2-bromopentane and 2-bromohexane were docked to the homology model of the enzyme. Since no difference in the binding energies of individual enantiomers was observed (data not shown), we could not gain further molecular details of the structural basis for low, but unusual, enantiopreference of this enzyme. Experimental determination of enzyme-substrate complexes using X-ray crystallography or nuclear magnetic resonance (NMR) spectroscopy would be the best way to get the necessary molecular details. However, trapping such complexes is extremely difficult for haloalkane dehalogenases, and no NMR structure has been solved even after many attempts made by other groups and by us.

Stopped-flow fluorescence analysis. The binding of bromide to DsvA, DsvA01, and DsvA02 was investigated by using stopped-flow fluorescence/anisotropy measurements. Fast binding kinetics of bromide occurred in the dead time of the instrument (1 ms) in the case of all tested DsvA variants. The signals of fluorescence intensity

(tryptophan quenching) and fluorescence anisotropy (tryptophan mobility change) reached rapid equilibrium and resulted in very similar equilibrium binding constants, which indicate specific binding interaction. The only difference observed was in the initial signal. The dissociation constants (K_d) calculated from the equilibrium levels of fluorescence intensity and fluorescence anisotropy obtained upon binding of bromide were 0.9 ± 0.1 M, 0.8 ± 0.2 M, and 1.3 ± 0.3 M for DsvAwt, DsvA01, and DsvA02, respectively (Table S4 and Fig. S6).

DISCUSSION

The present study describes the characterization of the novel haloalkane dehalogenase DsvA from the mildly thermophilic bacterium *S. viridis* strain DSM 43017. The phylogenetic and structural analyses of DsvA indicated the migration of the second halide-binding residue. DsvA contains phenylalanine (F165) in the canonical position of the second halide-stabilizing tryptophan, and a nearby tryptophan (W162) probably plays the role of the second halide-stabilizing residue. This proposal is further supported by the fact that the tryptophan-phenylalanine pair at the positions corresponding to W162 and F165 of DsvA was found in 23% of nonredundant sequences of the HLD-I subfamily, representing the second most common pair of residues at these positions after the phenylalanine-tryptophan pair (66% of nonredundant sequences).

A homology model of DsvA revealed that W162 was shifted one turn along the α-helix in the cap domain, and thus possibly provides for the stabilization of the halogen atom of the substrate from the opposite "mirrored" site compared to the typical position of the second halide-stabilizing residue of HLD-I members. To test this hypothesis, two single point mutations, F165W and W162F, and their combination (F165W+W162F) were introduced into the structure of DsvA. The resulting variants DsvA01, DsvA02, and DsvA03 were characterized together with the wild type, DsvAwt. The introduction of single point mutations did not affect the secondary structure or the stability of DsvA, whereas the combination of both mutations in DsvA03 decreased the enzyme stability by 5°C. While the F165W substitution in DsvA01 had no significant impact on the activity with 30 halogenated substrates, substitution W162F in DsvA02 reduced activity to 30 to 50%, confirming the importance of W162 for the enzyme catalysis. A similar drop in activity toward one representative substrate (1,2-dibromoethane) was also detected with DsvA03. An analogous result was previously obtained with DhlA, where a similar substitution of W175F, replacing the second halide-stabilizing residue, reduced the enzyme activity to 10 to 20% toward all tested substrates (11). Both single point mutants DsvA01 and DsvA02 exhibited the same substrate specificity as DsvAwt, and all variants were clustered into the substrate specificity group IV (SSG-IV), for which members preferentially convert terminally substituted brominated and iodinated compounds (30). A systematic comparison of the substrate specificities of individual HLDs within the phylogenetic tree revealed that the identified functional groups of enzymes are clearly distinct from the evolutionary subfamilies. This implies that the prediction of the substrate specificity of putative HLDs based on the sequence similarities with characterized family members is not currently possible (30).

An enantioselectivity measurement of DsvA performed with selected β-bromoalkanes uncovered a preference of the enzyme toward (*S*)-2-bromopentane and (*S*)-2-bromohexane over their (*R*)-enantiomers, which has never been observed for other characterized HLDs. We speculated that this unique enantiopreference could be a consequence of the unusual spatial arrangement of the second halide-stabilizing residue W162. However, introduced mutations modifying the arrangement of the halide-stabilizing residues caused only slight changes of enantioselectivity and did not switch enantiopreference with β-brominated alkanes. This suggests that additional structural features contribute to the (*S*)-preference of DsvA toward the β-bromoalkanes, which we did not affect by our mutagenesis. Previous investigation of the structural basis of enantioselectivity of highly selective HLDs DbjA (31) and DhaA31 (35) toward β-brominated alkanes uncovered that discrimination is either owing to the water-

promoted interactions of the substrate alkyl chain with the hydrophobic wall of the active site (in the case of DbjA) or owing to an occluded active site that spatially complements the preferred enantiomer of (*R*)-2-bromopentane (in the case of DhaA31).

In contrast, the enantioselectivity of DsvA for ethyl-2-bromopropionate and *N*-butyl-2-bromopropionamide was significantly affected by the introduced mutations. The introduction of F165W induced the ability of the enzyme to discriminate between the enantiomers of ethyl-2-bromopropionate and simultaneously decreased the enantioselectivity toward the amide. Replacement of the halide stabilizing W162 by F caused an even bigger drop in the enzyme enantioselectivity toward the amide, while retaining very low enantioselectivity toward the ester. Similar data were also observed after the introduction of both mutations (W162F+F165W) into DsvA03. This result provides further evidence for the involvement of W162 in substrate stabilization. It also correlates with the previously described molecular basis of DbjA enantioselectivity toward the α-brominated esters based on different interactions of individual enantiomers with the halide-stabilizing residues (31, 32). Both ethyl-2-bromopropionate and *N*-butyl-2-bromopropionamide can form an additional hydrogen bond of the carbonyl oxygen with side chains of halide-stabilizing residues. Modification of the halide-stabilizing residues had a more pronounced effect on DsvA enantioselectivity toward the α-bromoester and the α-bromoamide than on its enantioselectivity toward β-bromoalkanes.

Finally, the study of bromide binding by DsvA variants using a stopped-flow analysis provided a piece of direct evidence that W162 fulfills the function of a "conventional" halide-stabilizing residue in this enzyme. The experiments revealed that DsvA01 (F165W) has a similar affinity for bromide ions as DsvAwt, whereas DsvA02 (W162F) exhibited decreased affinity compared to DsvAwt. A modulated affinity was previously observed also for DhlA after substitution of its halide-stabilizing residue W175 with phenylalanine (11) or glutamine (15).

The unusual composition of halide-stabilizing residues was also observed for other HLD members. DmxA (17) from the HLD-II subfamily contains glutamine (Q40) instead of the usual asparagine. DmrB (18) from the HLD-III subfamily contains glutamic acid (E46) instead of asparagine as the halide-stabilizing residue. Both DmxA and DmrB are catalytically active, which suggests that a single primary halide-stabilizing residue is sufficient for substrate binding and halide ion stabilization. The importance of halide-stabilizing residues for the catalysis of DhlA was previously examined (9, 10). Kennes et al. (15) studied the role of W125 in DhlA and Krooshof et al. (11) investigated W175 in DhlA by site-directed mutagenesis. Bohac et al. (8) and Damborsky et al. (36) analyzed the importance of halide-stabilizing residues in the catalytic cycle of LinB and DhaA by quantum mechanics.

In summary, our study demonstrates that putative protein sequences with an unconventional composition of catalytic residues could be explored in genomic databases to identify novel HLD enzymes with unique catalytic properties.

MATERIALS AND METHODS

Identification of putative haloalkane dehalogenase. Sequences of three experimentally characterized HLDs (LinB (37), DhlA (38), and DrbA (22)) were used as queries for PSI-BLAST v2.2.28+ (39) searches against the nr database of NCBI (21). PSI-BLAST was conducted with the *E* value threshold of 10^{-20} for both the initial BLAST search and inclusion of the sequence in a position-specific matrix. Protein sequences collected after 2 iterations of PSI-BLAST were clustered with CLANS (40) using default parameters and various *P* value thresholds. Sequences clustered together with known HLDs at the *P* value of 10^{-40} were extracted. Information about the source organism of each putative HLD was collected from the BioProject database of NCBI (21) to identify sequences of thermophilic origin. The putative HLD from thermophilic bacterium *S. viridis* strain DSM 43017 (NCBI protein database accession number WP_012795647; referred to as DsvA) was selected for biochemical characterization.

Sequence alignment and construction of the homology model of DsvA. Sequences from the HLD-I subfamily (extracted from CLANS at the *P* value of 10^{-46}) were further clustered at 90% identity by the UCLAST method of the USEARCH program (41) to remove redundant sequences and aligned with Clustal Omega (42). The alignment was inspected in BioEdit (43). The homology model was constructed by SWISS-MODEL (44), using the structure of DmrA (RCSB PDB number 4MJ3) as the template, and visualized in PyMol (45). The template sequence identity of 55% (above the recommended 30% for

homology modeling), as well as the high resolution of the template structure (1.7 Å), guarantee acceptable reliability of the homology model. The homology model of DsvA was structurally aligned with DmrA to see the spatial arrangement of catalytic residues.

Gene synthesis and construction of mutants. The *dsvA* gene was synthesized (Mr. Gene, Germany), with the codon usage automatically adapted to the codon bias of *E. coli* genes. For expression purposes, the gene containing a C-terminal His tag was subcloned to the expression vector pET21b (Novagen, USA) between restriction sites NdeI and BamHI. The recombinant gene *dsva01* carrying mutation F165W was designed by an on-line algorithm developed by Agilent Technologies (USA) and constructed using QuikChange II side-directed mutagenesis kit (Agilent Technologies, USA) by PCR utilizing the mutagenic primer 5′-GCCGGAAGAATGGTGGGCATGGCGTGATGCAACCCAGAAAGC-3′ (underlining indicates the restriction site) and the nonmutagenic reverse primer pET_Rv 5′-AGACCCGTTTAGAGGCCCCAAGGGGTTATG-3′, following the method of Sanchis et al. (46). The gene *dsva02* carrying mutation W162F was designed using the online program One-Click using primer 1, 5′-CCGGAAGAATTTTGGGCATTTCGTGATGCAACCCAGAAAGCACCGG-3′, and primer 2, 5′-AAATGCCCAAAATTCTTCCGGCATTGCCTGATCACCTGTCGGCAGA-3′ (47). The gene *dsva03*, carrying mutations W162F+F165W, was designed using SnapGene Viewer 5.0.2 software (48) utilizing the *dsvA01* gene as a template and, for the introduction of the W162F mutation, employing the mutagenic primer 5′-GATCAGGCAATGCCGGAAGAATTTTGGGCATGGCGTGATGCAACCCAGAAAGCAC-3′. Template DNA was treated by DpnI endonuclease during 1 to 2 h of incubation at 37°C. Prepared plasmids pET21b::*dsvA*, pET21b::*dsvA01*, pET21b::*dsvA02*, and pET21b::*dsvA03* were transformed into *E. coli* DH5α cells. After overnight cultivation at 37°C, 3 to 6 colonies were picked from the agar plates and used for the preparation of 10-ml overnight cultures. Plasmids were isolated from the cultured cells using the GeneJET plasmid miniprep kit (Thermo Fisher Scientific, USA) and sequenced on both strands.

Protein expression and purification. To overproduce haloalkane dehalogenase DsvA and its variants in *E. coli*, the gene was expressed under the control of the T7 promoter and the gene expressions were induced by the addition of isopropyl β-D-1-thiogalactopyranoside (IPTG). *E. coli* BL21(DE3) cells containing recombinant plasmids pET21b::*dsvA*, pET21b::*dsvA01*, pET21b::*dsvA02*, and pET21b::*dsvA03* were grown in LB medium with ampicillin (100 $\mu g \cdot ml^{-1}$) at 37°C. When the culture reached an optical density at 600 nm (OD_{600}) of 0.6, the induction of enzyme expression (at 20°C) was initiated by the addition of IPTG to a final concentration of 0.5 mM. After overnight cultivation, the cells were harvested, disrupted by sonication using an ultrasonic processor UP200S (Hielscher, Germany), and centrifuged for 1 h at 4°C and 21,000 $\times$ *g*. DsvA and its variants were purified by Ni-NTA Superflow Cartridge (Qiagen, Germany). The His-tagged enzyme was bound to the resin in the equilibrating buffer (20 mM potassium phosphate buffer, pH 7.5, 0.5 M sodium chloride, 10 mM imidazole). Unbound and weakly bound proteins were washed out. The His-tagged enzyme was eluted by a buffer containing 300 mM imidazole. The eluted protein was pooled and dialyzed overnight against 50 mM potassium phosphate buffer (pH 7.5) and then stored at 4°C. The protein concentration was determined by the Bradford reagent (Sigma-Aldrich, USA) calibrated with bovine serum albumin (BSA), and the protein purity was checked by SDS-PAGE.

Circular dichroism spectroscopy and thermodynamic stability. Circular dichroism (CD) spectra of DsvA, DsvA01, DsvA02, and DsvA03 were recorded at 20°C using a Chirascan CD spectrometer (Applied Photophysics, United Kingdom). Data were collected from 180 to 260 nm, at 100 $nm \cdot min^{-1}$, 1 s response time, and 2 nm bandwidth using a 0.1 cm quartz cuvette containing 0.1 to 0.2 $mg \cdot ml^{-1}$ of the enzyme in 50 mM phosphate buffer pH 7.5. Presented spectra represent an average of five individual scans and have been corrected for baseline noise. CD data were expressed in terms of the mean residue ellipticity (Θ_{MRE}) using equation 1:

$$\Theta_{MRE} = \frac{\Theta_{obs} \cdot M_w \cdot 100}{n \cdot c \cdot l} \quad (1)$$

where Θ_{obs} is the observed ellipticity in degrees, M_w is the molecular weight, *n* is the number of residues, *l* is the cell path length, *c* is the enzyme concentration, and the factor 100 originates from the conversion of the molecular weight to $mg \cdot dmol^{-1}$.

The thermal unfolding of DsvA and its variants was followed by monitoring the ellipticity at 221 nm over the temperature range from 20°C to 80°C, with a resolution 0.1°C and a heating rate of $1°C \cdot min^{-1}$. Recorded thermal denaturation curves were normalized to represent signal changes between approximately 1 and 0 and fitted to sigmoidal curves using software Origin 6.1 (OriginLab, USA). The apparent melting temperature ($T_{m,app}$) was evaluated as an inflection point of normalized thermal transition.

Substrate specificity and principle-component analysis. The specific activity of DsvA toward 30 halogenated substrates was assayed by the method of Iwasaki et al. (49). The release of halide ions was measured spectrophotometrically at 460 nm using the microplate reader Sunrise (Tecan, Austria) after reaction with mercuric thiocyanate and ferric ammonium sulfate. The dehalogenation reactions were performed at 37°C in 25-ml Reacti-flasks closed by Mininert valves. The reaction mixtures consisted of 10 ml of 100 mM glycine buffer pH 8.6 and 10 μl of an appropriate substrate in a concentration between 0.1 and 10 mM, depending on the substrate solubility. The reactions were initiated by the addition of 0.05 to 0.3 ml of the enzyme in the concentration of 0.3 to 6 $mg \cdot ml^{-1}$. The reactions were monitored by withdrawing 1-ml samples at periodic intervals from the reaction mixture and immediately mixing with 0.1 ml of 35% nitric acid to terminate the reaction. The spontaneous hydrolysis of substrates in buffer was tested in the abiotic control. Dehalogenation activity data, measured in three to five independent replicates, were quantified as the rate of product formation in time after the subtraction of spontaneous hydrolysis.

The data matrix containing the specific activities for DsvA, DsvA01, DsvA02, and HLDs DhlA, DhaA, DbjA, LinB, DmbA, DbeA (30), DmbC, DrbA (22), DmxA (17), DatA (33), and DpcA (24) toward 30 halogenated substrates was analyzed by the multidimensional statistical method principal-component analysis (PCA) using the Statistica 10.0 software package (StatSoft, USA) as described previously by Koudelakova et al. (30). The individual enzymes were considered as cases, whereas their substrates as variables. The raw data were log-transformed and weighted relative to the individual enzyme's activity toward other substrates prior to analysis in order to better discern individual enzymes' specificity profiles. These transformed data were used to position DsvA within the predefined substrate specificity groups (SSGs).

Enantioselectivity. The enantioselectivity measurement was performed at 20°C in 25-ml Reactiflasks closed by Mininert valves containing 25 ml of 100 mM glycine buffer pH 8.6. The racemic substrates 2-bromopentane, 2-bromohexane, ethyl-2-bromopropionate, and *N*-butyl-2-bromopropionamide were added to the reaction mixture to a final concentration of 0.5 to 1.2 mM. The reaction was initiated by the addition of 0.1 to 1 ml of an enzyme (2.5 to 15.0 mg · ml^{-1}) into the reaction mixture. The reaction progress was monitored by periodical withdrawing of 0.5 ml samples from the reaction mixture. The samples were mixed with methanol (reactions with 2-bromohexane) or diethyl ether (experiments with 2-bromopentane, ethyl-2-bromopropionate, and *N*-butyl-2-bromopropionamide) containing 1,2-dichloroethane as an internal standard. The samples extracted in diethyl ether were analyzed with a Hewlett-Packard 6890 gas chromatograph (Agilent, USA) equipped with a flame ionization detector and chiral capillary column Chiraldex G-TA and B-TA (Alltech, USA). The samples mixed with methanol were analyzed with an Agilent Technologies 7890A gas chromatograph (Agilent, USA) equipped with a flame ionization detector and chiral capillary column Astec Chiraldex B-DM (50 m by 0.25 mm by 0.12 μl film thickness) (Sigma-Aldrich, USA). The enantioselectivity was expressed as an *E* value, defined as the ratio between the specificity constants (k_{cat}/K_m) for the two enantiomers (equation 2):

$$E = \frac{k_{cat}^{R}/K_{m}^{R}}{k_{cat}^{S}/K_{m}^{S}} \quad (2)$$

where k_{cat} and K_m represent the Michaelis–Menten parameters of the enzyme with the two enantiomers. The equations describing the competitive Michaelis-Menten kinetics (50) were fitted by numerical integration to progress curves obtained from the kinetic resolution experiments with the software Scientist (MicroMath Research, USA) to estimate the kinetic parameters. Enantiopreference of DsvA variants toward 2-bromopentane and 2-bromohexane was determined by comparison of retention times and gas chromatography-mass spectrometry (GC-MS) spectra between the produced alcohol or remaining substrate enantiomer with enantiopure standards (Sigma-Aldrich, USA).

Molecular docking. The three-dimensional structures of 2-bromopentane and 2-bromohexane were taken from our in-house database and converted into the Sybyl mol2 file format using OpenBabel (51). The model was further converted by MGLTools (52) into AutoDock Vina (53) compliant pdbqt format. The constructed homology model of DsvA was used as the target for molecular docking. Hydrogen atoms were added to the target using H++ webserver (54) at pH 7.5. The Gasteiger charges and AutoDock atom types were assigned to target by MGLTools (52). AutoDock Vina was used for the identification of the ligand-binding orientations in the active site of the enzyme. The docking box of AutoDock Vina had a size of 17.5 by 17.5 by 17.5 Å, and the search space was centered at the catalytic nucleophile to cover the whole active site and the main tunnel of the receptor. AutoDock Vina (53) was used with default settings except of increased exhaustiveness to 30 for better sampling. All clusters with negative binding energy were manually inspected in PyMOL (45) to assess if they are binding in a near attack conformation (NAC) typical for an S_N2 reaction. The following geometrical parameters were measured: (i) the distance between the ligand's halogen atom and polar hydrogens of both halide-stabilizing residues (W162 and W125, respectively); (ii) the distance between the halogen-substituted atom on the ligand and D124 OD2 atom; and (iii) the angle between halogen, the C, and D124 OD2 atom.

Stopped-flow fluorescence analysis. Binding experiments were performed in an SFM-300 stopped-flow instrument (BioLogic, France) combined with a MOS-500 spectropolarimeter. The fluorescence emission from tryptophan residues was observed through a 320-nm cutoff filter upon excitation at 295 nm. The reactions were performed at 37°C in a glycine buffer pH 8.6 by rapid mixing of 15 μM enzyme with bromide to a final concentration of 0 to 2 M. Dissociation constants were determined from the dependence of steady-state fluorescence and anisotropy on bromide concentration by using the Stern-Volmer equation (equation 3):

$$\frac{F}{F_0} = \frac{1 + f \cdot K_a \cdot [Br^-]}{1 + K_a \cdot [Br^-]} \quad (3)$$

where $[Br^-]$ is a concentration of bromide ion, F/F_0 is the relative fluorescence, *f* is the fluorescence level of the ligand-bound enzyme, and K_a is the association equilibrium constant of specific binding of bromide into the enzyme (the dissociation constant $K_d = 1/K_a$) (55). Nonlinear regression fitting was performed with the software Origin 6.1 (OriginLab, USA).

SUPPLEMENTAL MATERIAL

Supplemental material is available online only.

SUPPLEMENTAL FILE 1, PDF file, 2.3 MB.

ACKNOWLEDGMENTS

The authors express sincere thanks to Martin Marek (Masaryk University, Brno, Czech Republic) for valuable comments on the manuscript.

This work was supported by the Grant Agency of the Czech Republic (17-24321S), the Ministry of Education, Youth, and Sports of the Czech Republic (LQ1605, CZ.02.1.01/0.0/0.0/16_013/0001761, LM2015047, LM2015055), and the European Union (720776, 722610, 814418).

REFERENCES

1. Janssen DB. 2004. Evolving haloalkane dehalogenases. Curr Opin Chem Biol 8:150–159. https://doi.org/10.1016/j.cbpa.2004.02.012.
2. Damborsky J, Rorije E, Jesenska A, Nagata Y, Klopman G, Peijnenburg WJ. 2001. Structure-specificity relationship for haloalkane dehalogenases. Environ Toxicol Chem 20:2681–2689. https://doi.org/10.1002/etc.5620201205.
3. Verschueren KHG, Seljée F, Rozeboom HJ, Kalk KH, Dijkstra BW. 1993. Crystallographic analysis of the catalytic mechanism of haloalkane dehalogenase. Nature 363:693–698. https://doi.org/10.1038/363693a0.
4. Ollis DL, Cheah E, Cygler M, Dijkstra BW, Frolow F, Franken SM, Harel M, Remington SJ, Silman I, Schrag J, Sussman JL, Verschueren KHG, Goldman A. 1992. The alpha/beta hydrolase fold. Protein Eng 5:197–211. https://doi.org/10.1093/protein/5.3.197.
5. Nardini M, Dijkstra BW. 1999. Alpha/beta hydrolase fold enzymes: the family keeps growing. Curr Opin Struct Biol 9:732–737. https://doi.org/10.1016/S0959-440X(99)00037-8.
6. Holmquist M. 2000. Alpha/beta-hydrolase fold enzymes: structures, functions and mechanisms. Curr Protein Pept Sci 1:209–235. https://doi.org/10.2174/1389203003381405.
7. Chovancova E, Kosinski J, Bujnicki MJ, Damborsky J. 2007. Phylogenetic analysis of haloalkane dehalogenases. Proteins 67:305–316. https://doi.org/10.1002/prot.21313.
8. Bohac M, Nagata Y, Prokop Z, Prokop M, Monincova M, Tsuda M, Koca J, Damborsky J. 2002. Halide-stabilizing residues of haloalkane dehalogenases studied by quantum mechanic calculations and site-directed mutagenesis. Biochemistry 41:14272–14280. https://doi.org/10.1021/bi026427v.
9. Verschueren KH, Kingma J, Rozeboom HJ, Kalk KH, Janssen DB, Dijkstra BW. 1993. Crystallographic and fluorescence studies of the interaction of haloalkane dehalogenase with halide ions. Studies with halide compounds reveal a halide binding site in the active site. Biochemistry 32:9031–9037. https://doi.org/10.1021/bi00086a008.
10. Schindler JF, Naranjo PA, Honaberger DA, Chang CH, Brainard JR, Vanderberg LA, Unkefer CJ. 1999. Haloalkane dehalogenases: steady-state kinetics and halide inhibition. Biochemistry 38:5772–5778. https://doi.org/10.1021/bi982853y.
11. Krooshof GH, Ridder IS, Tepper AW, Vos GJ, Rozeboom HJ, Kalk KH, Dijkstra BW, Janssen DB. 1998. Kinetic analysis and X-ray structure of haloalkane dehalogenase with a modified halide-binding site. Biochemistry 37:15013–15023. https://doi.org/10.1021/bi9815187.
12. Schanstra JP, Kingma J, Janssen DB. 1996. Specificity and kinetics of haloalkane dehalogenase. J Biol Chem 271:14747–14753. https://doi.org/10.1074/jbc.271.25.14747.
13. Pikkemaat MG, Ridder IS, Rozeboom HJ, Kalk KH, Dijkstra BW, Janssen DB. 1999. Crystallographic and kinetic evidence of a collision complex formed during halide import in haloalkane dehalogenase. Biochemistry 38:12052–12061. https://doi.org/10.1021/bi990849w.
14. Prokop Z, Monincova M, Chaloupkova R, Klvana M, Nagata Y, Janssen DB, Damborsky J. 2003. Catalytic mechanism of the haloalkane dehalogenase LinB from *Sphingomonas paucimobilis* UT26. J Biol Chem 278:45094–45100. https://doi.org/10.1074/jbc.M307056200.
15. Kennes C, Pries F, Krooshof GH, Bokma E, Kingma J, Janssen DB. 1995. Replacement of tryptophan residues in haloalkane dehalogenase reduces halide binding and catalytic activity. Eur J Biochem 228:403–407. https://doi.org/10.1111/j.1432-1033.1995.0403n.x.
16. Carlucci L, Zhou E, Malashkevich VN, Almo SC, Mundorff EC. 2016. Biochemical characterization of two haloalkane dehalogenases: DccA from *Caulobacter crescentus* and DsaA from *Saccharomonospora azurea*. Protein Sci 25:877–886. https://doi.org/10.1002/pro.2895.
17. Chrast L, Tratsiak K, Planas-Iglesias J, Daniel L, Prudnikova T, Brezovsky J, Bednar D, Kuta Smatanova I, Chaloupkova R, Damborsky J. 2019. Deciphering the structural basis of high thermostability of dehalogenase from psychrophilic bacterium *Marinobacter* sp. ELB17. Microorganisms 7:498. https://doi.org/10.3390/microorganisms7110498.
18. Fung HK, Gadd MS, Drury TA, Cheung S, Guss JM, Coleman NV, Matthews JM. 2015. Biochemical and biophysical characterisation of haloalkane dehalogenases DmrA and DmrB in *Mycobacterium* strain JS60 and their role in growth on haloalkanes. Mol Microbiol 97:439–453. https://doi.org/10.1111/mmi.13039.
19. Pati A, Sikorski J, Nolan M, Lapidus A, Copeland A, Glavina Del Rio T, Lucas S, Chen F, Tice H, Pitluck S, Cheng J-F, Chertkov O, Brettin T, Han C, Detter JC, Kuske C, Bruce D, Goodwin L, Chain P, D'haeseleer P, Chen A, Palaniappan K, Ivanova N, Mavromatis K, Mikhailova N, Rohde M, Tindall BJ, Göker M, Bristow J, Eisen JA, Markowitz V, Hugenholtz P, Kyrpides NC, Klenk H-P. 2009. Complete genome sequence of *Saccharomonospora viridis* type strain (P101). Stand Genomic Sci 1:141–149. https://doi.org/10.4056/sigs.20263.
20. Greiner-Mai E, Korn-Wendisch F, Kutzner HJ. 1988. Taxonomic revision of the genus *Saccharomonospora* and description of *Saccharomonospora glauca* sp. nov. Int J Syst Bacteriol 38:398–405. https://doi.org/10.1099/00207713-38-4-398.
21. Sayers EW, Barrett T, Benson DA, Bolton E, Bryant SH, Canese K, Chetvernin V, Church DM, Dicuccio M, Federhen S, Feolo M, Fingerman IM, Geer LY, Helmberg W, Kapustin Y, Krasnov S, Landsman D, Lipman DJ, Lu Z, Madden TL, Madej T, Maglott DR, Marchler-Bauer A, Miller V, Karsch-Mizrachi I, Ostell J, Panchenko A, Phan L, Pruitt KD, Schuler GD, Sequeira E, Sherry ST, Shumway M, Sirotkin K, Slotta D, Souvorov A, Starchenko G, Tatusova TA, Wagner L, Wang Y, Wilbur WJ, Yaschenko E, Ye J. 2012. Database resources of the National Center for Biotechnology Information: update. Nucleic Acids Res 40:D13–D25. https://doi.org/10.1093/nar/gkr1184.
22. Jesenska A, Monincova M, Koudelakova T, Hasan K, Chaloupkova R, Prokop Z, Geerlof A, Damborsky J. 2009. Biochemical characterization of haloalkane dehalogenases DrbA and DmbC, representatives of a novel subfamily. Appl Environ Microbiol 75:5157–5160. https://doi.org/10.1128/AEM.00199-09.
23. Christenson JK, Robinson SL, Engel TA, Richman JE, Kim AN, Wackett LP. 2017. OleB from bacterial hydrocarbon biosynthesis is a β-lactone decarboxylase that shares key features with haloalkane dehalogenases. Biochemistry 56:5278–5287. https://doi.org/10.1021/acs.biochem.7b00667.
24. Drienovska I, Chovancova E, Koudelakova T, Damborsky J, Chaloupkova R. 2012. Biochemical characterization of a novel haloalkane dehalogenase from a cold-adapted bacterium. Appl Environ Microbiol 78:4995–4998. https://doi.org/10.1128/AEM.00485-12.
25. Kodicek M, Karpenko V. 2000. Physical biochemistry, p 283–294. Academia, Prague.
26. Koudelakova T, Bidmanova S, Dvorak P, Pavelka A, Chaloupkova R, Prokop Z, Damborsky J. 2013. Haloalkane dehalogenases: biotechnological applications. Biotechnol J 8:32–45. https://doi.org/10.1002/biot.201100486.
27. Fortova A, Sebestova E, Stepankova V, Koudelakova T, Palkova L, Damborsky J, Chaloupkova R. 2013. DspA from *Strongylocentrotus purpuratus*: the first biochemically characterized haloalkane dehalogenase of non-microbial origin. Biochimie 95:2091–2096. https://doi.org/10.1016/j.biochi.2013.07.025.
28. Buryska T, Babkova P, Vavra O, Damborsky J, Prokop Z. 2017. A haloalkane dehalogenase from a marine microbial consortium possessing exceptionally broad substrate specificit. Appl Environ Microbiol 84:e01684-17. https://doi.org/10.1128/AEM.01684-17.

29. Vanacek P, Sebestova E, Babkova P, Bidmanova S, Daniel L, Dvorak P, Stepankova V, Chaloupkova R, Brezovsky J, Prokop Z, Damborsky J. 2018. Exploration of enzyme diversity by integrating bioinformatics with expression analysis and biochemical characterization. ACS Catal 8:2402–2412. https://doi.org/10.1021/acscatal.7b03523.
30. Koudelakova T, Chovancova E, Brezovsky J, Monincova M, Fortova A, Jarkovsky J, Damborsky J. 2011. Substrate specificity of haloalkane dehalogenases. Biochem J 435:345–354. https://doi.org/10.1042/BJ20101405.
31. Prokop Z, Sato Y, Brezovsky J, Mozga T, Chaloupkova R, Koudelakova T, Jerabek P, Stepankova V, Natsume R, van Leeuwen JG, Janssen DB, Florian J, Nagata Y, Senda T, Damborsky J. 2010. Enantioselectivity of haloalkane dehalogenases and its modulation by surface loop engineering. Angew Chem Int Ed Engl 49:6111–6115. https://doi.org/10.1002/anie.201001753.
32. Chaloupkova R, Prokop Z, Sato Y, Nagata Y, Damborsky J. 2011. Stereoselectivity and conformational stability of haloalkane dehalogenase DbjA from *Bradyrhizobium japonicum* USDA110: the effect of pH and temperature. FEBS J 278:2728–2738. https://doi.org/10.1111/j.1742-4658.2011.08203.x.
33. Hasan K, Fortova A, Koudelakova T, Chaloupkova R, Ishitsuka M, Nagata Y, Damborsky J, Prokop Z. 2011. Biochemical characteristics of the novel haloalkane dehalogenase DatA, isolated from the plant pathogen *Agrobacterium tumefaciens* C58. Appl Environ Microbiol 77:1881–1884. https://doi.org/10.1128/AEM.02109-10.
34. Westerbeek A, Szymański W, Wijma HJ, Marrink SJ, Feringa BL, Janssen DB. 2011. Kinetic resolution of α-bromoamides: experimental and theoretical investigation of highly enantioselective reactions catalyzed by haloalkane dehalogenases. Adv Synth Catal 353:931–944. https://doi.org/10.1002/adsc.201000726.
35. Liskova V, Stepankova V, Bednar D, Brezovsky J, Prokop Z, Chaloupkova R, Damborsky J. 2017. Different structural origins of the enantioselectivity of haloalkane dehalogenases toward linear β-haloalkanes: open-solvated versus occluded-desolvated active sites. Angew Chem Int Ed Engl 56:4719–4723. https://doi.org/10.1002/anie.201611193.
36. Damborsky J, Kuty M, Nemec M, Koca J. 1997. A molecular modeling study of the catalytic mechanism of haloalkane dehalogenase: 1. Quantum chemical study of the first reaction step. J Chem Inf Comput Sci 37:562–568. https://doi.org/10.1021/ci960483j.
37. Nagata Y, Miyauchi K, Damborsky J, Manova K, Ansorgova A, Takagi M. 1997. Purification and characterization of a haloalkane dehalogenase of a new substrate class from a gamma-hexachlorocyclohexane-degrading bacterium, *Sphingomonas paucimobilis* UT26. Appl Environ Microbiol 63:3707–3710. https://doi.org/10.1128/AEM.63.9.3707-3710.1997.
38. Keuning S, Janssen DB, Witholt B. 1985. Purification and characterization of hydrolytic haloalkane dehalogenase from *Xanthobacter autotrophicus* GJ10. J Bacteriol 163:635–639. https://doi.org/10.1128/JB.163.2.635-639.1985.
39. Altschul SF, Madden TL, Schäffer AA, Zhang J, Zhang Z, Miller W, Lipman DJ. 1997. Gapped BLAST and PSI-BLAST: a new generation of protein database search programs. Nucleic Acids Res 25:3389–3402. https://doi.org/10.1093/nar/25.17.3389.
40. Frickey T, Lupas A. 2004. CLANS: a Java application for visualizing protein families based on pairwise similarity. Bioinformatics 20:3702–3704. https://doi.org/10.1093/bioinformatics/bth444.
41. Edgar RC. 2010. Search and clustering orders of magnitude faster than BLAST. Bioinformatics 26:2460–2461. https://doi.org/10.1093/bioinformatics/btq461.
42. Sievers F, Wilm A, Dineen D, Gibson TJ, Karplus K, Li W, Lopez R, McWilliam H, Remmert M, Soding J, Thompson JD, Higgin DG. 2011. Fast, scalable generation of high-quality protein multiple sequence alignments using Clustal Omega. Mol Syst Biol 7:539. https://doi.org/10.1038/msb.2011.75.
43. Hall TA. 1999. BioEdit: a user-friendly biological sequence alignment editor and analysis program for Windows 95/98/NT. Nucleic Acids Symp Ser (Oxf) 41:95–98.
44. Waterhouse A, Bertoni M, Bienert S, Studer G, Tauriello G, Gumienny R, Heer FT, de Beer TAP, Rempfer C, Bordoli L, Lepore R, Schwede T. 2018. SWISS-MODEL: homology modelling of protein structures and complexes. Nucleic Acids Res 46:W296–W303. https://doi.org/10.1093/nar/gky427.
45. Schrodinger, LLC. 2020. The PyMOL molecular graphics system, version 2.0. Schrodinger, LLC, Portland, OR.
46. Sanchis J, Fernández L, Carballeira JD, Drone J, Gumulya Y, Höbenreich H, Kahakeaw D, Kille S, Lohmer R, Peyralans JJ, Podtetenieff J, Prasad S, Soni P, Taglieber A, Wu S, Zilly FE, Reetz MT. 2008. Improved PCR method for the creation of saturation mutagenesis libraries in directed evolution: application to difficult-to-amplify templates. Appl Microbiol Biotechnol 81:387–397. https://doi.org/10.1007/s00253-008-1678-9.
47. Warburton M, Omar Ali H, Liong WC, Othusitse AM, Zubir A, Maddock S, Wong TS. 2015. OneClick: a program for designing focused mutagenesis experiments. AIMS Bioeng 2:126–143. https://doi.org/10.3934/bioeng.2015.3.126.
48. GSL Biotech. 2020. SnapGene Viewer 5.0.2. GSL Biotech, Chicago, IL.
49. Iwasaki I, Utsumi S, Ozawa T. 1952. New colorimetric determination of chloride using mercuric thiocyanate and ferric ion. BCSJ 25:226–226. https://doi.org/10.1246/bcsj.25.226.
50. Lutje Spelberg JH, Rink R, Kellogg RM, Janssen DB. 1998. Enantioselectivity of a recombinant epoxide hydrolase from *Agrobacterium radiobacter*. Tetrahedron Asymm 9:459–466. https://doi.org/10.1016/S0957-4166(98)00003-2.
51. O'Boyle NM, Banck M, James CA, Morley C, Vandermeersch T, Hutchison GR. 2011. Open Babel: an open chemical toolbox. J Cheminform 3:33. https://doi.org/10.1186/1758-2946-3-33.
52. Morris GM, Huey R, Lindstrom W, Sanner MF, Belew RK, Goodsell DS, Olson AJ. 2009. AutoDock4 and AutoDockTools4: automated docking with selective receptor flexibility. J Comput Chem 30:2785–2791. https://doi.org/10.1002/jcc.21256.
53. Trott O, Olson AJ. 2010. AutoDock Vina: improving the speed and accuracy of docking with a new scoring function, efficient optimization, and multithreading. J Comput Chem 31:455–461. https://doi.org/10.1002/jcc.21334.
54. Anandakrishnan R, Aguilar B, Onufriev AV. 2012. H++ 3.0: automating pK prediction and the preparation of biomolecular structures for atomistic molecular modeling and simulations. Nucleic Acids Res 40:W537–W541. https://doi.org/10.1093/nar/gks375.
55. Stern O, Volmer M. 1919. Über die Abklingungszeit der Fluoreszenz. Phys Zeitschrift 20:183–188.